Dynamic Buckling Characteristics of Elastic Shell under Torsional Deformation

IOP Conf. Series: Earth and Environmental Science **560** (2020) 012013 doi:10.1088/1755-1315/560/1/012013

Dynamic Buckling Characteristics of Elastic Shell under Torsional Deformation

WX Zhang[1*], XW Hu[2]

[1] Nantong Polytechic College, Nantong, Jiangsu, 226002, China

[2]School of Civil and Environmental Engineering, Hunan University of Science and Engineering, Yongzhou, Hunan, 425199, China

[*]Corresponding author's e-mail: Wxzhang697608@sina.com

Abstract. In order to solve the dynamic buckling problem of elastic cylindrical shell under torsional impact, the original and dual variables of the problem are constructed by means of the energy of the system, and the Hamiltonian system of the system is established. According to the characteristics of Hamiltonian regular equation and symplectic space, the initial boundary value problem of partial differential equation is transformed into an algebraic equation problem by using the boundary conditions and compatibility conditions expressed by dual variables, and the analytical expressions of symplectic eigenvalues and eigensolutions are obtained.

1. Introduction

At present, the measurement technology is more mature, which is the most commonly used method. However, this method can only measure the deformation history of a certain point in the structure, so the deformation information of the whole field can not be obtained. High speed photography is to use high-speed camera to photograph the whole modal change process of the structure in the dynamic buckling process. [1-3] The high-speed photography can record the clear images of the configuration in each stage of the dynamic buckling process of the structure. Although this method can get a series of whole field configurations of time structure, it is discrete in time coordinate, often only do some qualitative analysis, but not quantify it. Therefore, these two methods are usually combined in experiments.

In recent years, with the continuous development and improvement of photomechanics, it is possible to apply new experimental techniques and methods to the experimental study of structural dynamic buckling [4-7]. Image moire method is a new measurement and control method of stress and strain. It overcomes the shortcoming that electrical measurement can only measure point by point, and can give the whole field deformation information. The dynamic moire photograph contains rich deformation technology. It can not only give the stress-strain information of the buckling movement of the structure, determine the characteristic parameters of the buckling, but also provide a new experimental method for the post buckling theory. Of course, due to the limitations of experimental conditions and techniques, the application of dynamic moire technology in the experimental study of structural dynamic buckling is still difficult. In this paper, by virtue of the properties and completeness of Hamiltonian system, a complete space of buckling modes is given, and the corresponding relationship between the critical loads and buckling modes in symplectic system is revealed.

2. Solution method

Under the condition of torsion, the deformation potential energy density, bending potential energy density and kinetic energy density are

$$\Pi_{\varepsilon} = \frac{1}{2}K(\varepsilon_x^2 + \varepsilon_\theta^2 + 2\upsilon\varepsilon_x\varepsilon_\theta + \frac{1-\upsilon}{2}\varepsilon_{x\theta}^2) + \frac{N_{x\theta}}{r}\partial_x w\cdot\partial_\theta w \tag{1}$$

$$\Pi_k = \frac{1}{2}D(\kappa_x^2 + \kappa_\theta^2 + 2\upsilon\kappa_x\kappa_\theta + 2(1-\upsilon)\kappa_{x\theta}^2) \tag{2}$$

and

$$\Pi_t = \frac{1}{2}\rho h(\frac{\partial u}{\partial t})^2 + \frac{1}{2}\rho h(\frac{\partial v}{\partial t})^2 + \frac{1}{2}\rho h(\frac{\partial w}{\partial t})^2 \tag{3}$$

respectively. Because the thickness diameter ratio of the shell is very small, the Lagrangian function and the Hamiltiona funnction can be written as

$$\begin{aligned} L = \iint\{&\frac{1}{2}\rho h(\frac{\partial u}{\partial t})^2 + \frac{1}{2}\rho h(\frac{\partial v}{\partial t})^2 + \frac{1}{2}\rho h(\frac{\partial w}{\partial t})^2 - \frac{1}{2}K(\varepsilon_x^2 + \varepsilon_\theta^2 + 2\upsilon\varepsilon_x\varepsilon_\theta + \frac{1-\upsilon}{2}\varepsilon_{x\theta}^2) - \\ &\frac{1}{2}D[\kappa_x^2 + \kappa_\theta^2 + 2\upsilon\kappa_x\kappa_\theta + 2(1-\upsilon)\kappa_{x\theta}^2] - \frac{N_{x\theta}}{r}\partial_x w\cdot\partial_\theta w\} r d\theta dx \end{aligned} \tag{4}$$

and

$$H(\mathbf{q},\mathbf{p}) = \mathbf{p}^{\mathrm{T}}\dot{\mathbf{q}} - L(\mathbf{q},\mathbf{p}) = -\frac{Eh}{2r^2}w^2 + \frac{1}{2D}p_2^2 - p_1\varphi_\theta + p_2 w'' - N_{x\theta}w'\varphi_\theta \tag{5}$$

Applying the Hamiltonian variational principle, we have

$$\begin{aligned} \delta\iiint\{&\frac{\rho h}{2}(\partial_t v)^2 - \frac{(1-\upsilon)K}{4}(\partial_x v)^2 - \frac{Eh}{2r^2}w^2 - \frac{D}{2}[(\partial_x^2 w)^2 + \frac{1}{r^4}(\partial_\theta^2 w)^2 + \\ &\frac{2\upsilon}{r^2}(\partial_x^2 w)(\partial_\theta^2 w) + \frac{2(1-\upsilon)}{r^2}(\partial_x\partial_\theta w)^2] - \frac{N_{x\theta}}{r}\partial_x w\cdot\partial_\theta w] r d\theta dx dt = 0 \end{aligned} \tag{6}$$

respectively. Therefore, we deduce the following Hamiltonian regular equations

$$\dot{\psi} = \mathbf{H}\psi \tag{7}$$

where

$$\psi = \{q^T \; p^T\} = \{w, \phi_\theta, p_1, p_2\} \tag{8}$$

and

$$H = \begin{bmatrix} 0 & -1 & 0 & 0 \\ \partial_x^2 & 0 & 0 & 1/D \\ \frac{Eh}{r^2} & -N_{x\theta}\partial_x & 0 & -\partial_x^2 \\ N_{x\theta}\partial_x & 0 & 1 & 0 \end{bmatrix} \tag{9}$$

The final solution of Eq. (7) can be obtained as

$$\varphi_n(x) = \sum_{k=1}^{4} C_k e^{\eta_k x} \begin{Bmatrix} 1 \\ -in/r \\ D(in^3/r^3 + \eta_k n^2/r^2) \\ D(n^2/r^2 - \eta_k^2) \end{Bmatrix} \tag{10}$$

The displacement component is

$$w(x,\theta) = \sum_{n=0}^{\infty} \left[a_n e^{\eta_k x}\ e^{in\theta} + b_n e^{-\eta_k x}\ e^{-in\theta} \right] = \sum_{n=0}^{\infty} \left(a_n e^{\eta_k + in\theta} + b_n e^{-\eta_k - in\theta} \right) \tag{11}$$

3. Numerical results

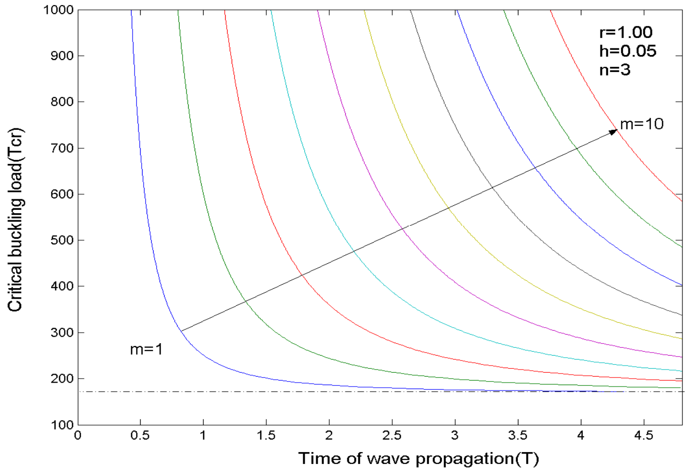

Figure 1. The first ten branches of critical buckling loads.

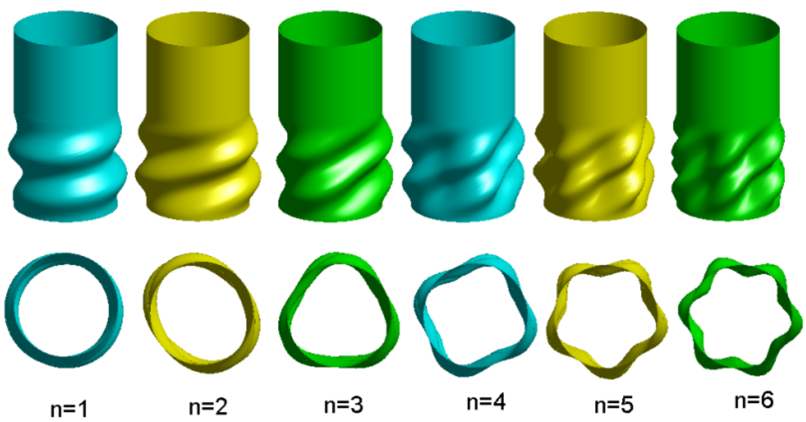

Figure 2. The first six orders of critical buckling modes.

Fig.1 shows the first ten critical buckling load curves. It can be seen that at the beginning of the torsional impact load, the critical buckling load of the shell decreases rapidly with the propagation of the axial stress wave. Fig.2 depicts the critical buckling modes corresponding to different orders. The results indicate that there is no axisymmetric buckling for torsional impact buckling, and the buckling stages is non axisymmetric.

Acknowledgments
This research was financially supported by Major Natural Science Research Projects in Colleges and Universities of Jiangsu Province (17KJA430012).

References

[1] Micallef, K., Sagaseta, J., Ruiz, M.F., Muttoni, A. (2013) Assessing punching shear failure in reinforced concrete flat slabs subjected to localised impact loading. Int. J. Impact Eng., 71: 17-33.
[2] Azimi, M.B., Asgari M. (2016) A new bi-tubular conical-circular structure for improving crushing behavior under axial and oblique impacts. Int. J. Mech. Sci., 105: 253-265.
[3] Greiner, R., Guggenberger, W. (1998) Buckling behavior of axially loaded steel cylinders on local supports-with and without internal pressure. Thin Wall. Struct., 31: 159-167.
[4] Priza, K., Wijeyewickrema, A.C., Kikuo, K. (2011) Wave propagation along a non-principal direction in a compressible pre-stressed elastic layer. Int. J. Solid. Struct., 48: 2141-2153.
[5] Leyko, L., Spryzynski, S. (1974) Energy method of analysis of dynamic stability of cylindrical shells subjected to torsion. Arch. Mech., 26: 13-24.
[6] Tan, D.Y. (2000) Torsional buckling analysis of thin and thick shells of revolution. Int. J. Solid. Struct., 37: 3055-3078.
[7] Mao, R.J., Lu, G.A. (2002) Study of elastic-plastic buckling of cylindrical shells under torsion. Thin Wall. Struct., 40: 1051-1071.